Interatomic potential for vanadium suitable for radiation damage simulations

Seungwu Han, Luis A. Zepeda-Ruiz, Graeme J. Ackland, Roberto Car, and David J. Srolovitz

Citation: Journal of Applied Physics **93**, 3328 (2003); doi: 10.1063/1.1555275
View online: http://dx.doi.org/10.1063/1.1555275
View Table of Contents: http://scitation.aip.org/content/aip/journal/jap/93/6?ver=pdfcov
Published by the AIP Publishing

Interatomic potential for vanadium suitable for radiation damage simulations

Seungwu Han
Princeton Materials Institute, Princeton University, Princeton, New Jersey 08544

Luis A. Zepeda-Ruiz
Princeton Materials Institute and Department of Mechanical and Aerospace Engineering, Princeton University, Princeton, New Jersey 08544

Graeme J. Ackland
Department of Physics and Astronomy, University of Edinburgh, Edinburgh EH9 3JZ, Scotland, United Kingdom

Roberto Car
Princeton Materials Institute and Department of Chemistry, Princeton University, Princeton, New Jersey 08544

David J. Srolovitz[a)]
Princeton Materials Institute and Department of Mechanical and Aerospace Engineering, Princeton University, Princeton, New Jersey 08544

(Received 5 September 2002; accepted 6 January 2003)

The ability to predict the behavior of point defects in metals, particularly interstitial defects, is central to accurate modeling of the microstructural evolution in environments with high radiation fluxes. Existing interatomic potentials of embedded atom method type predict disparate stable interstitial defect configurations in vanadium. This is not surprising since accurate first-principles interstitial data were not available when these potentials were fitted. In order to provide the input information required to fit a vanadium potential appropriate for radiation damage studies, we perform a series of first-principles calculations on six different interstitial geometries and vacancies. These calculations identify the $\langle 111 \rangle$ dumbbell as the most stable interstitial with a formation energy of approximately 3.1 eV, at variance with predictions based upon existing potentials. Our potential is of Finnis–Sinclair type and is fitted exactly to the experimental equilibrium lattice parameter, cohesive energy, elastic constants and a calculated unrelaxed vacancy formation energy. Two additional potential parameters were used to obtain the best fit to the set of interstitial formation energies determined from the first-principles calculations. The resulting potential was found to accurately predict both the magnitude and ordering of the formation energies of six interstitial configurations and the unrelaxed vacancy ground state, in addition to accurately describing the migration characteristics of the stable interstitial and vacancy. This vanadium potential is capable of describing the point defect properties appropriate for radiation damage simulations as well as for simulations of more common crystal and simple defect properties. [DOI: 10.1063/1.1555275]

I. INTRODUCTION

Vanadium-based alloys are among the candidate structural materials for use in future fusion reactors.[1] These alloys combine several appealing properties: they do not readily become radioactive under a 14 MeV neutron flux, they exhibit good strength at elevated temperatures, are compatible with liquid lithium and exhibit a high thermal stress factor (low thermal expansion and elastic modulus). As a result, these materials have received considerable experimental and theoretical attention.[2] Modeling of radiation damage must account for radiation-induced microstructural evolution that leads to severe degradation of a wide range of important mechanical properties and significant dimensional changes. A comprehensive modeling program must be inherently multiscale (both in space and time) since the evolution is mediated by a combination of atomic level dynamics, defect physics, nonequilibrium thermodynamics and transport kinetics.[3,4] The simulations at larger scales must be parameterized either using data obtained from experiment or from simulations on the smaller scales. Hence, the multiscale simulation framework rests on the reliability of the atomistic simulation results. At a minimum, atomistic simulations must be able to reproduce the structure and energetics of the point defects that are present in the irradiated material, in addition to the perfect crystal properties. The point defect properties are of particular interest in these materials since their production, migration and annihilation control the radiation-induced swelling, yield strength and ductility of metallic alloys in such applications.

The reliability of the atomistic simulations depends largely on the accuracy of the modeled atomic interactions.

a)Electronic mail: srol@princeton.edu

TABLE I. Formation energies (in eV) of several types of interstitials from existing EAM/FS interatomic potentials (the sources of the potentials are the references in column 1).

Reference	⟨100⟩ dumbbell	⟨110⟩ dumbbell	⟨111⟩ dumbbell	⟨111⟩ crowdion	Octahedral
18	4.58	4.90	4.78	···	4.64
19	4.96	4.16	4.61	4.60	···
21	4.24	4.80	5.21	4.06	···

While first-principles methods constitute the most reliable approach to determining atomic interactions, application of these methods to systems with more than a few hundred atoms is not feasible. Most atomistic simulations of defects in metals are performed using semiempirical or empirical descriptions of atomic interactions, such as tight binding methods,[5] bond order potentials,[6] embedded-atom-method (EAM) potentials,[7,8] Finnis–Sinclair[9] (FS) potentials, or simple pair potentials. Each approach represents a different trade-off between errors due to small simulation size and inaccurate forces. While simple pair potentials are often capable of predicting some crystalline properties, they also have some dramatic shortcomings that arise from their oversimplistic form in predicting the sign of the surface relaxation, in reproducing the experimental Cauchy pressure $(C_{12}-C_{44})/2$, and in predicting some defect properties.[10,11] EAM/FS many-body potentials have been proven to be widely applicable to surfaces,[7,12] vacancies,[13,14] phonon spectra,[15] dislocations,[16] and alloy properties.[17] Most of the recent atomistic radiation damage (cascade) simulation have used potentials of EAM/FS type, which are both computationally efficient and provide a reasonable description of many types of crystal defects. Typically, potentials of this type are fit to bulk properties (lattice parameter, cohesive energy, elastic constants) and to the vacancy formation energy.

Because interstitial properties have not previously been included in the fitting procedure for most EAM/FS potentials, it is not surprising that different EAM/FS potentials yield widely disparate predictions for the energetics of self-interstitials in vanadium as well as the structure of the stable interstitial,[18,19,20] as shown in Table I. This failure may be traced to the fact that the minimum interatomic separation near interstitials is much smaller than the equilibrium nearest neighbor spacing in a perfect crystal and that the atomic rearrangements are very anisotropic close to the interstitials. This deficiency arises because of the dearth of experimental data for self-interstitials: they are present in large quantities only in irradiated specimens.[21] One approach by which to address these deficiencies is to obtain accurate predictions of point defect properties from first-principles methods and use these in the fitting procedure for the interatomic potential. First-principles calculations can also be used to provide reliable predictions of self-interstitial properties that can be used in molecular dynamics and kinetic Monte Carlo studies of point defect evolution in irradiated materials.[22] First-principles calculation of self-interstitial properties for iron have been reported previously.[23] The large lattice distortions associated with self-interstitials imply that accurate first-principles calculations of interstitial properties will require some of the largest calculation cells ever used.

In this study, we describe the procedure employed to fit an interatomic potential for vanadium that is suitable for radiation damage simulations, report this potential, and compare predictions made using this potential to first-principles results and experiments. We first report the results of systematic first-principles calculations of point defects (self-interstitials and vacancies) in vanadium. Several different possible self-interstitial structures were investigated to determine which is stable and to provide additional data to be used in the potential fitting procedure. In addition to fitting to both point defect formation and migration energies, we fit to perfect crystal data (lattice parameter, cohesive energy, elastic constants). Simulations performed with this potential confirm that it reproduces both perfect crystal properties and point defect formation energies. In addition, we use the potential to determine phonon spectra and to determine the activation energy for diffusion and the threshold displacement energy for neutron irradiation of vanadium (i.e., the minimum kinetic energy of a neutron required to produce stable point defects) using moledular dynamics.

II. FIRST-PRINCIPLES METHOD

Within the density functional pseudopotential framework,[24] the total energy of a system with a given ionic configuration is expressed in atomic units ($m_e=1$, $\hbar=1$, $e=1$) as

$$\begin{aligned} E_{\text{tot}} &= E_{\text{kinetic}} + E_{\text{el-ion}} + E_{\text{el-el}}^{\text{Hartree}} + E_{XC} + E_{\text{ion-ion}} \\ &= \sum_{\mathbf{k}} \sum_{i}^{\text{occp}} \left\langle \psi_{i,\mathbf{k}} \left| -\frac{1}{2}\nabla^2 + V_{\text{ion}} \right| \psi_{i,\mathbf{k}} \right\rangle \\ &\quad + \frac{1}{2} \int \frac{\rho(\mathbf{r})\rho(\mathbf{r}')}{|\mathbf{r}-\mathbf{r}'|} d\mathbf{r} d\mathbf{r}' \\ &\quad + \int \epsilon_{XC}[\rho(\mathbf{r}), \nabla\rho(\mathbf{r})]\rho(\mathbf{r}) d\mathbf{r} + \frac{1}{2} \sum_{I \neq J} \frac{Z_I Z_J}{|R_I - R_J|} \end{aligned} \tag{1}$$

$$\rho(\mathbf{r}) = \sum_{\mathbf{k}} \sum_{i}^{\text{occp}} \langle \psi_{i,\mathbf{k}} | \psi_{i,\mathbf{k}} \rangle, \tag{2}$$

where R_I and Z_I are coordinates and ionic charges of the Ith atom, respectively. $\psi_{i,\mathbf{k}}$ is a valence pseudowave function corresponding to the ith band at the $\mathbf{k}$ point in the Brillouin zone (BZ). For the exchange-correlation energy density ϵ_{XC}, which reflects the quantum many-body interaction of the

TABLE II. Comparison of the equilibrium properties of vanadium obtained via first-principles calculations and experiment. Values in parentheses refer to calculations performed at the experimental lattice parameter. $3s3p$ core ($3s3p$ valence) refers to our pseudopotential results where the $3s$ and $3p$ electrons are not included (or included) in the valence. FLAPW is an all-electron calculation.

	$3s3p$ core	$3s3p$ valence	FLAPW[a]	FLAPW[b]	Experiment[c]
a_0 (Å)	2.99(3.02)	3.00(3.02)	3.00	2.99	3.02
B (eV/Å^3)	1.20	1.14	1.12	1.23	0.999
dB/dP	4.1	3.8	3.8	⋯	⋯
C_{11} (eV/Å^3)	1.69(1.49)	1.61(1.44)	⋯	⋯	1.43
C_{12} (eV/Å^3)	0.949(0.824)	0.887(0.787)	⋯	⋯	0.743
C_{44} (eV/Å^3)	0.137(0.131)	0.125(0.112)	⋯	⋯	0.269

[a]Reference 30.
[b]Reference 31.
[c]Reference 32.

electrons, we use the generalized gradient approximation (GGA) with the functional form developed by Perdew *et al.*[25]

A plane wave basis is used to expand the wave function:

$$\psi_{i,\mathbf{k}}(\mathbf{r}) = \sum_{\mathbf{G}} c_{i,\mathbf{k}}(\mathbf{G}) e^{i(\mathbf{k}+\mathbf{G})\cdot\mathbf{r}}, \tag{3}$$

where summation over the **G** vectors is bounded by the energy cutoff (E_{cut}) in such a way that $|\mathbf{k}+\mathbf{G}|^2 < 2E_{\text{cut}}$. For the electron–ion interaction represented by V_{ion}, we use an ultrasoft pseudopotential[26] which has good transfer properties while requiring only a relatively small energy cutoff for plane wave expansion of the valence orbitals. In pseudopotential formalism, the core electrons which do not contribute to interatomic bonding are implicitly included in repulsive interaction near the core. This dramatically accelerates the computation by reducing the number of electrons that has to be treated explicitly in the calculation. Including plane waves with kinetic energy less than 408 eV ensures convergence of the total energy to within 0.02 eV/atom in crystalline vanadium. In generating the pseudopotential, we employ the $3d^3 4s^2 4p^0$ valence electron configuration while underlying core electrons are frozen. We use one projector for each s and p orbital and two projectors for each d orbital in order to accurately describe the d bands. The cutoff radii employed for the ionic potential are 1.13, 1.34, and 0.95 Å for the s, p, and d channels, respectively. We include nonlinear core corrections[27] in the exchange-correlation energy to account for the interaction between valence and core charges.

The computer package PWSCF[28] was used for the first-principles calculations. This program not only calculates the electronic structure at a given ionic configuration but also relaxes the atomic coordinates as well as the size and shape of the simulation cell. In our calculations, we optimize the atomic positions until the Hellmann–Feynman forces are less than 5×10^{-2} eV/Å. Damped cell dynamics[29] are used to relax lattice vectors and we ensure that all components of the average stress tensor are less than 5×10^{-4} eV/Å^3. As a simple test of the method, we calculate several bulk properties of vanadium (see Table II). The lattice parameter, bulk modulus, and its derivative are obtained by fitting the energy–volume curve to Birch's equation of state.[33] The elastic constants are obtained from the stress–strain relation,[34] i.e., we apply $\pm1\%$ strain and calculate the resultant stress tensor. The values in parentheses in Table II are evaluated at the experimental equilibrium lattice parameter. To estimate the errors inherent in the pseudopotential, we generate another pseudopotential for which the $3s$ and $3p$ orbitals are removed from the core and treated as valence electrons. Table II also shows a comparison of our pseudopotential results with all-electron (FLAPW) calculations[31,32] and experiment.[33] Overall, the agreement between the elastic constants C_{ij} and the bulk modulus B from the calculations and experiment (and other reference calculations) is quite good except for C_{44} which shows relatively large deviation from experiment. The agreement in the elastic constants is improved when the calculations are performed at the experimental lattice parameter, indicating that the errors in the elastic constants are associated to a large extent with underestimation of the lattice parameter.

III. POINT DEFECT ENERGIES IN VANADIUM

A. Self-interstitials

Figure 1 shows a schematic illustration of the six high-symmetry self-interstitials that we examined via first-principles calculations. Before considering the relative energies of these different configurations, we first examine the convergence of the formation energy with respect to supercell size in a system containing a single ⟨111⟩-dumbbell interstitial. The supercell consists of a simple cubic arrange-

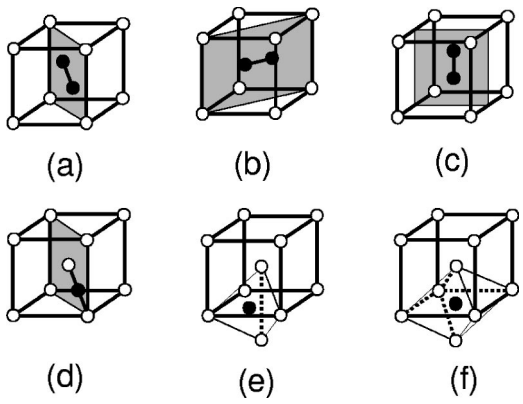

FIG. 1. Schematic illustration of possible interstitials: (a) ⟨111⟩, (b) ⟨110⟩, and (c) ⟨100⟩ dumbbells, (d) crowdion, (e)tetrahedral, and (f) octahedral.

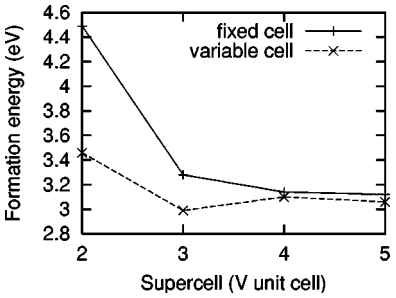

FIG. 2. Variation of the ⟨111⟩-dumbbell self-interstitial formation energy E_I^f with the linear dimension of the cubic supercell. In fixed cell data, the internal coordinates of the atoms are fully relaxed but the cell size and shape are fixed, whereas in variable cell data, both the internal coordinates and the size/shape of the cell are relaxed.

ment of $m\times m\times m$ body-centered-cubic (bcc) unit cells ($2m^3$ atoms). The supercell is periodically repeated in space to represent an infinite, perfect crystal. The defect formation energy is obtained from the difference in system energy with and without an interstitial:

$$E_I^f = E_{\text{tot}}(N+1) - \frac{N+1}{N} E_{\text{tot}}(N), \tag{4}$$

where N is the number of atoms in the perfect crystal and $N+1$ in the system with an interstitial. Figure 2 shows the variation of the formation energy E_I^f of the ⟨111⟩-dumbbell self-interstitial with respect to the linear dimension of the supercell. More details of these calculations are provided in Table III. The supercell containing 251 atoms is one of the largest transition metal systems ever examined via first-principles methods. Figure 2 suggests that E_I^f converges to within 0.05 eV for supercells larger than $3\times3\times3$ (i.e., at least 129 atoms). Although relaxation of the cell shape significantly lowers E_I^f, this type of relaxation gives an underestimate of the formation energy at large supercell sizes, whereas the fixed cell calculations lead to an overestimate of E_I^f. If the relaxation of the supercell were purely dilational, the elastic energy of this relaxation would be $E_{\text{el}} = V_0 P^2/2B$, where V_0 is the equilibrium volume and P is the pressure found in the fixed supercell calculation. Examination of Table III shows that E_{el} provides a measure of the effect of the supercell size on E_I^f. The overall convergence of the first-principles calculation in Table III is faster than in studies with empirical potentials[35,36] (see also below), where typically thousands of atoms are included in the supercell. A similar convergence check for the ⟨100⟩-dumbbell self-interstitial also suggests that a $4\times4\times4$ supercell is sufficient to ensure convergence to within 0.05 eV (see Table III).

Table IV shows the interstitial formation energies E_I^f for all of the interstitials in Fig. 1 evaluated with the fixed-volume $4\times4\times4$ supercell. The stable self-interstitial in V is either a ⟨111⟩ dumbbell or a crowdion. The very small difference in energy ($\lesssim$0.01 eV) between the ⟨111⟩ dumbbell and the crowdion is beyond the accuracy of density functional calculations. The prediction that the ⟨111⟩ dumbbell is the most stable interstitial contradicts earlier results obtained using EAM/FS potentials.[18,19,20] The ⟨110⟩ dumbbell, which is the most stable interstitial in some of the EAM studies, has the third smallest formation energy. Furthermore, the predicted magnitude of E_I^f (3.14 eV) is well below that found in previous EAM/FS calculations (4.61–4.78 eV).

The physics underlying the relative values of E_I^f for the ⟨111⟩, ⟨110⟩, ⟨100⟩ dumbbells can be understood by examining the type of strain produced by these differently oriented dumbbells. In each case, the predominant deformation is uniaxial strain along the direction of symmetry of the dumbbell. This suggests that the modulus associated with uniaxial strain in the direction of the dumbbell, $M_{\langle ijk\rangle}$, should be correlated with the formation energy. This is confirmed in Table V which shows that theoretical and experimental values of $M_{\langle ijk\rangle}$ are exactly of the same order as the E_I^f of the corresponding dumbbell (see Table IV).

No direct experimental data exist from which we can determine the symmetry of the self-interstitial in V. However, it is well known from radiation-damage experiments that the migration barrier of the self-interstitial is very small ($<$0.01 eV) and that diffusion occurs even at 4 K.[37] The first-principles data, presented above, suggest that the lowest activation energy migration path for the ⟨111⟩ dumbbell corresponds to a transformation from a ⟨111⟩ dumbbell to a crowdion (i.e., the transition state) before and then back again to a ⟨111⟩ dumbbell. The diffusion barrier for this path is simply the difference in E_I^f between the ⟨111⟩ dumbbell and the crowdion configuration. As shown in Table IV, this energy is very small ($\sim$0.01 eV), consistent with experiment. Interestingly, these results suggest that at low temperatures, self-interstitial diffusion should be one dimensional (along the ⟨111⟩ direction). The transition state for rotation from a given ⟨111⟩ direction to another corresponds to the ⟨110⟩-dumbbell configuration. Therefore, the activation en-

TABLE III. Convergence of E_I^f for the ⟨111⟩-dumbbell self-interstitial in V with respect to the supercell size. $E_I^f(1)$ and $E_I^f(2)$ indicate the formation energy for the fixed and relaxed cells, respectively. E_{el} is the elastic energy assuming dilational relaxation of the supercell. $N_{\mathbf{k}}$ is the number of $\mathbf{k}$ points sampled in the first BZ. The energies and pressure (P) are in eV and GPa, respectively. We define the pressure as minus one third of the trace of the stress tensor for the fixed cell. $\Delta E_I^f\,[=E_I^f(1)-E_I^f(2)]$ indicates the change in the formation energy when the cell is relaxed. For comparison, the convergence of the ⟨100⟩ dumbbell is shown in the last column.

Supercell size	N_{atom}	$N_{\mathbf{k}}$	$E_I^f(1)$	P	E_{el}	$E_I^f(2)$	ΔE_I^f	$E_I^f(1)$[100]
$2a_0\times2a_0\times2a_0$	16(+1)	64	4.49	17.3	0.80	3.46	1.03	5.86
$3a_0\times3a_0\times3a_0$	54(+1)	27	3.28	4.6	0.23	2.99	0.29	3.91
$4a_0\times4a_0\times4a_0$	128(+1)	8	3.14	1.4	0.06	3.10	0.04	3.57
$5a_0\times5a_0\times5a_0$	250(+1)	8	3.12	0.5	0.01	3.06	0.06	3.57

TABLE IV. The formation energies of the interstitials in Fig. 1.

	⟨100⟩ dumbbell	⟨110⟩ dumbbell	⟨111⟩ dumbbell	⟨111⟩ crowdion	Octahedral	Tetrahedral
E_I^f	3.57	3.48	3.14	3.15	3.62	3.69

ergy for dumbbell rotation should be 0.44 eV (see Table IV). This suggests that at a sufficiently high temperature, the dumbbell should exhibit three-dimensional diffusion.

B. Monovacancy

Unlike the self-interstitial, a monovacancy creates relatively small simple (i.e., centro symmetric) distortion. A $3\times3\times3$ supercell is sufficient to study the isolated monovacancy when relaxing both internal coordinates and supercell size/shape. We used 4 **k** points in the irreducible BZ wedge. Earlier studies on vacancies in tantalum[38] and tungsten[39] suggest that this is sufficient to obtain adequate convergence for the formation energy. The vacancy formation energy E_V^f can be computed as

$$E_V^f = E_{\text{tot}}(N-1) - \frac{N-1}{N} E_{\text{tot}}(N), \tag{5}$$

where $E_{\text{tot}}(N-1)$ and $E_{\text{tot}}(N)$ are the total energies of the system with and without a vacancy, respectively. Our calculated formation energy is 2.6 eV of which 0.07 eV comes from the volume relaxation. This is within the error bar of the experimentally determined vacancy formation energy, 2.2 ± 0.4 eV.[40] By assuming that the transition state is midway between two nearest neighbor atom positions along the ⟨111⟩ direction, we estimate the monovacancy migration energy as 0.33 eV, which is close to the estimated experimental value of 0.5 eV.[40]

IV. INTERATOMIC POTENTIALS

A. Fitting method

A surprising result of the first-principles calculations is that the self-interstitial formation energy is much smaller than previously predicted on the basis of atomistic simulations using EAM/FS potentials (cf. Tables I and IV). These potentials modeled the nearest neighbor approach using the high pressure data from electronic structure calculations[19] or from the ''universal equation of state.''[41] Such input data correspond to purely hydrostatic deformation (i.e., one that equally compresses all eight bonds around each atom), while deformation along a ⟨111⟩ dumbbell is more closely uniaxial (i.e., corresponding to compressing only two opposing bonds). The implication is that it is more than eight times harder to compress eight neighboring atom bonds together than it is to compress two. This can, in turn, be traced to a fundamental misconception in fitting empirical potentials, namely, that the short range repulsion is due to pairwise overlap of core electrons. This can be clearly seen in the predictions of pseudopotential calculations which specifically exclude this effect, and show that the energy cost of compression arises primarily from the increased kinetic energy of the electrons. This observation does not, of course, invalidate previous potentials. Rather, it is essentially a transfer problem, and merely indicates that we should not expect a potential fitted to high pressure data to perform well in applications involving the close approach of atoms without hydrostatic compression of the lattice. In EAM/FS formalism, this suggests that some of the resistance to compression is intrinsically many body, and so for the study of defect fitting should be done to interstitial energy rather than to high pressure data.

TABLE V. Theoretical values for the moduli associated with uniaxial strain, $M_{\langle111\rangle}=(C_{11}+2C_{12}+4C_{44})/3$, $M_{\langle110\rangle}=(C_{11}+C_{12})/2+C_{44}$, and $M_{\langle100\rangle}=C_{11}$, where C_{11}, C_{12}, and C_{44} are the elastic constants of the vanadium single crystal. Units are in eV/Å^3.

	$M_{\langle111\rangle}$	$M_{\langle110\rangle}$	$M_{\langle100\rangle}$
Theory	1.38	1.46	1.69
Experiment	1.33	1.35	1.43

For this work, we parameterized a potential for vanadium following FS formalism of the second-moment approximation to tight-binding theory, which is valid for *d*-band transition metals where charge transfer is unimportant.[42] The basic equation for the energy of an atom (i) is given by[43]

$$E_i = \tfrac{1}{2}\sum_j V(r_{ij}) - \rho_i^{1/2}, \tag{6}$$

where

$$\rho_i = \sum_j \phi(r_{ij}). \tag{7}$$

We use a cubic spline representation of the functions $V(r_{ij})$ and $\phi(r_{ij})$ given by

$$V(r) = \sum_{k=1}^{6} a_k (r_k - r)^3 H(r_k - r), \tag{8}$$

$$\phi(r) = \sum_{k=1}^{2} A_k (R_k - r)^3 H(R_k - r), \tag{9}$$

where r_k and R_k are knot points such that $r_1>r_2>r_3>r_4>r_5>r_6$ and $R_1>R_2$. $H(x)$ is the Heaviside step function; $H(x)=0$ for $x<0$ and $H(x)=1$ for $x>0$. We fit six parameters (the r_k and R_k are fixed) exactly[44] to reproduce the three cubic elastic constants, the cohesive energy, the lattice parameter and the unrelaxed vacancy formation energy of vanadium. These quantities are summarized in Table VI.

The fit to the vacancy formation energy was made for the energy of an unrelaxed vacancy using a Taylor expansion for the many-body part ($E_V^{f,u}$), and subtracted from the cohesive energy. Assuming the range extends to second neighbors $[x_1=(\sqrt{3}/2)a_0;\ x_2=a_0]$ this has an analytic form of

$$E_{\text{coh}} - E_V^{f,u} = 14\sqrt{8\phi(x_1)+6\phi(x_2)} - 8\sqrt{7\phi(x_1)+6\phi(x_2)} - 6\sqrt{8\phi(x_1)+5\phi(x_2)}, \tag{10}$$

$$\approx \frac{1}{2}\sqrt{8\phi(x_1)+6\phi(x_2)}. \tag{11}$$

TABLE VI. Data used to fit the vanadium potential. The elastic moduli are from compilation by Simmons and Wang (Ref. 45), and the unrelaxed vacancy formation energy and the cohesive energy are from the present first-principles calculations.

Quantity	a (Å)	$E_{\rm coh}$ (eV)	C_{11} (eV/Å^3)	C_{12} (eV/Å^3)	C_{44} (eV/Å^3)	$E_V^{f,u}$ (eV)
Value	3.03	5.3	1.42	0.743	0.269	2.85

Only after the potential has been constructed is it possible to fully relax the vacancy. With previous vanadium potentials[19] the relaxation energy has been about 0.25 eV. We assumed a similar value would apply here, so we set $E_V^{f,u}=E_V^f+0.25$ eV for fitting, taking $E_V^f=2.6$ eV from the first-principles data. We take the value of $E_{\rm coh}$ from the calorimetric data.[46] The Cauchy pressure $C_{12}-C_{44}$ also depends on the many-body term only, and with $E_{\rm coh}-E_V^{f,u}$ it provides a set of two linear equations for A_1 and A_2. The equilibrium value of ρ is fully determined by the difference between $E_V^{f,u}$ and $E_{\rm coh}$: $\rho_0=2(E_{\rm coh}-E_V^{f,u})^2$. This is true for any EAM model when the ''squared'' operator is replaced by the inverse of the embedding operator. Once A_1 and A_2 are fit, the other quantities have a linear dependence on a_i.

With six constraints satisfied exactly, the problem is reduced to determining the two remaining free parameters, which we took to be the value of the ''effective'' potential $[V(r_{ij})-\phi(R_{ij})/\sqrt{\rho_0}]$ at the nearest neighbor separation and the value of a_6. These were adjusted to give the best fit to the difference in energy between bcc and face-centered-cubic (fcc) structures,[47] correct ordering of the interstitial formation energy, the relaxation energy of the vacancy and the high pressure equation of state. The relaxation energy of the interstitials is much larger than that for the vacancy and, in the case of dumbbells, the ''unrelaxed'' state cannot be uniquely defined because the dumbbell separation is arbitrary. Similarly, the lattice parameter of the fcc phase was not fitted because it is not possible to express the fcc formation energy analytically.

The fact that a reasonable fit to all these data can be obtained with two parameters indicates that fitting the first six quantities captures much of the physics of vanadium. A similar result was obtained for iron.[48] The fitted coefficients are compiled in Table VII.

B. Point defect properties

The properties of the relaxed point defects were determined by minimizing the total energy with respect to all atomic coordinates using a conjugate-gradient method. Periodic boundary conditions were employed and the simulation cell size was varied to ensure that the formation energies were independent of the cell size to the desired accuracy (0.01 eV). The convergence of E_I^f with the simulation cell size using this potential is shown in Fig. 3. The variable cell E_I^f converges to the asymptotic value from below, while that for the fixed cell converges from above, as observed in the first-principles results in Fig. 2. The saturation of the formation energy occurs at a slightly larger supercell than that for the corresponding first-principles calculation.

Table VIII shows the resultant point defect formation energies in vanadium. Excellent agreement between the formation energies using the present potentials and first-principles results was obtained in all cases (i.e., within 5% or 0.18 eV). As in the first-principles results, the ⟨111⟩ dumbbell and ⟨111⟩ crowdion are degenerate in energy and represent the most stable self-interstitial configurations. This result is in contrast with that obtained using other EAM/FS interatomic potentials (shown in Table I), which show a variety of stable self-interstitial configurations. As for the first-principles results, the self-interstitial formation energies determined here are approximately 1 eV lower in energy compared with predictions made using other potentials. For additional comparison, the distance between two atoms that compose a dumbbell is reported in Table IX for high-symmetry self-interstitials. The agreement is within 5% and it is even better when data are scaled by the lattice parameter in each theoretical approach.

Perhaps a more sensitive test of the quality of the interatomic potential is its ability to predict kinetic parameters, such as the activation energies for point defect migration. The activation energies for vacancy migration determined from the present potential, from first-principles calculations, and estimated from experimental data[42] are 0.42, 0.33, and 0.5 eV, respectively. The activation energies for ⟨111⟩-dumbbell self-diffusion determined using this potential and first-principles are 0.04 and 0.01 eV, respectively, while the experimental value is less than 0.01 eV (Ref. 39) (recall in Sec. III A that the first-principles results are not accurate for energies smaller than approximately 0.05 eV). Three-dimensional diffusion requires rotation of the ⟨111⟩ dumbbell from one ⟨111⟩ direction to another. The activation energy for such a rotation is 0.41 and 0.34 eV based upon the potential and first-principles calculations. In all of these cases, the agreement is very good, especially given the limits of accuracy of the first-principles calculations and the uncer-

TABLE VII. Fitted coefficients for the present vanadium potential [Eqs. (8) and (9)]. r_k and R_k are in units of the bcc lattice parameter (a_0) while coefficients a_k and A_k are in eV/a_0^3 and eV^2/a_0^6, respectively. In order to simulate primary knock-on events, modification of the short range potential to, e.g., the Biersack form (Refs. 48 and 50) is used.

r_1	1.300 000	a_1	−71.861 297
r_2	1.220 000	a_2	221.019 869
r_3	1.150 000	a_3	−203.133 261
r_4	1.060 000	a_4	118.249 184
r_5	0.950 000	a_5	−93.678 070
r_6	0.866 025	a_6	141.643 266
R_1	1.300 000	A_1	26.834 293
R_2	1.200 000	A_2	6.118 468

TABLE VIII. Comparison of the formation energies of point defects in vanadium obtained using the Finnis–Sinclair potential fitted here and first-principles results. Energies are in eV.

	Vacancy	⟨100⟩ dumbbell	⟨110⟩ dumbbell	⟨111⟩ dumbbell	⟨111⟩ crowdion	Octahedral	Tetrahedral
First principles	2.60	3.57	3.48	3.14	3.15	3.62	3.69
FS (present)	2.63	3.60	3.66	3.27	3.27	3.60[a]	3.64

[a]Unstable configuration; decays to a ⟨100⟩ dumbbell.

tainty in the experimental data. Preliminary displacement cascade simulations performed using the present interatomic potential in a molecular dynamics (MD) simulation have shown that the vast majority of the point defects generated were vacancies and ⟨111⟩-dumbbell self-interstitials.[49] This is consistent with the predictions made above based upon static relaxation using the potential (and first principles). Additional MD simulations show the transition from one-dimensional ⟨111⟩-dumbbell diffusion at low temperature to three-dimensional ⟨111⟩-dumbbell diffusion at high temperature. These MD simulations further demonstrate that the present potential yields reasonable high temperature properties.

C. Phonon spectrum

We have calculated the phonon spectrum that corresponds to the present potential.[51] We use the second derivative of the potential to evaluate force constants and dynamical matrices.[52] The many-body form of the potential introduces several extra terms into the force constants which extends their effective range to double that of the potential.[9] In principle, this could be used to fit the phonon spectrum, but here no information about the phonons was included in the fitting process so the dispersion relation provides a severe test, although for use in radiation-damage simulations precise harmonic phonons near the zone boundaries are not crucial. Figure 4 show the predicted dispersion, calculated at 0 K compared with the room temperature data from thermal diffuse scattering of x rays.[53] In general, the potential is slightly too soft, but the main discrepancy appears to be at the *H* point, where the potential underestimates the experimental value by 30%. Some of this can be attributed to thermal effects, and the underestimate seems to be typical of other similar potentials.[18]

V. CONCLUSIONS

Modern multiscale modeling of radiation-damage phenomena relates atomic scale molecular dynamics simulation of cascades to point defect production and migration which, in turn, feeds into kinetic Monte Carlo and rate equation modeling of the temporal evolution of point defect distributions, and finally to the prediction of evolving mechanical properties through dislocation dynamics and constitutive modeling. The results of such modeling can be no better than its foundation. In many cases, this foundation is atomistic modeling based upon empirical or semiempirical descriptions of the underlying atomic interactions. The embedded-atom method and FS potentials have become the most common form of interatomic potentials used in large-scale atomistic simulations of metals. These potentials are typically fit to the properties of the perfect crystal and to vacancy formation energies. As such, no data are included in the fit on length scales much below that of the nearest neighbor spacing in the perfect crystal. On the other hand, radiation damage is based upon collision cascades that typically produce interstitials, with nearest neighbor spacings which are considerably smaller. Therefore, it is not surprising that different interatomic potentials can lead to very different results for the properties of point defects that are central to prediction of radiation damage. Moreover, fitting the short range interaction from high pressure data incorporates different physics from those required for interstitials, typically resulting in excessively high formation energies.

In order to build interatomic potentials appropriate for radiation-damage studies in vanadium, we performed a series of first-principles calculations designed to determine which types of interstitials are stable in V and to determine the relative formation energies of competing point defects. These large-scale first-principles calculations clearly show that the most stable type of interstitial is either a ⟨111⟩ dumbbell or ⟨111⟩ crowdion, rather than the ⟨110⟩ dumbbell, ⟨100⟩ dumbbell, or octahedral or tetrahedral interstitials. Further, these calculations also explained the large extent of interstitial diffusion observed at very low temperature in vanadium.[37] This diffusion occurs via a one-dimensional random walk process in which the interstitials move from ⟨111⟩-dumbbell to ⟨111⟩-crowdion positions with an extremely low activation barrier, while at high temperature, rotations of the ⟨111⟩ dumbbell

TABLE IX. Comparison of the atomic separations of a dumbbell from first-principles calculations and the present FS potentials. Units are in Å.

	⟨100⟩	⟨110⟩	⟨111⟩
First principles	2.159	2.076	2.124
FS (present)	2.103	2.167	2.190

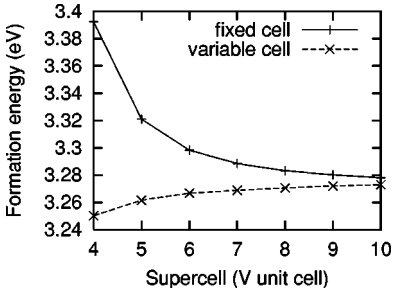

FIG. 3. Convergence of E_I^f with the supercell size for the ⟨111⟩ dumbbell using the potential developed here.

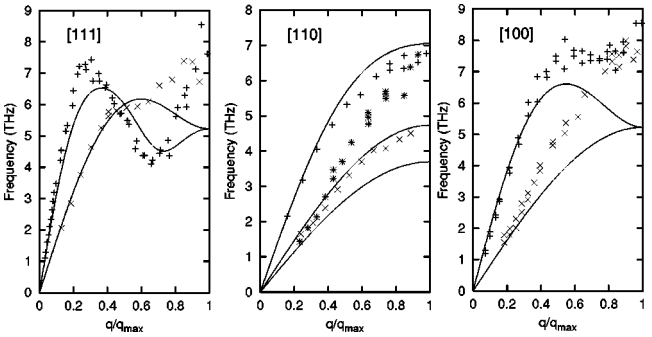

FIG. 4. Phonon spectrum along the high-symmetry axis calculated with the FS potential. $q_{\max}$ is π/a for [111] and [110], and $2\pi/a$ for [100].

from one orientation to another occur, giving rise to three-dimensional diffusion.

The present FS type of potential was fit exactly to the experimental values of the equilibrium lattice parameter, cohesive energy, and three elastic constants and an estimated unrelaxed vacancy formation energy and two parameters were used to obtain the best fit to the set of interstitial formation energies determined from the first-principles calculations. The potential was modified at very short ranges to ensure the appropriate form for primary knock-on events. The resultant potential was then tested by comparing the heats of formation of six interstitial configurations and a vacancy obtained using the potential and from first principles. The agreement is uniformly excellent (to within the accuracy of the first-principles calculations), both in the magnitude of the energies and in the relative ordering of the competing structures. Further, the ⟨111⟩-dumbbell migration and rotation energies and the vacancy migration energy also show excellent correspondence between the calculations performed with the potential, with the first-principles method, and from experiment (where available). The ability to predict the seven point defect interstitial formation energies and the three migration energies without decreasing the quality of the fit to the perfect crystal data with only two additional parameters demonstrates the robustness of the present potential. This vanadium is capable of describing the point defect properties appropriate for radiation-damage simulations as well as for simulations of more common crystal and simple defect properties.

ACKNOWLEDGMENTS

The authors gratefully acknowledge useful discussions with M. Baskes, S. Srinivasan, B. Wirth, S. Dudarev, D. Pettifor and A. Sutton. The computation was carried out at NERSC and the Keck Materials Science Computing Center at Princeton. One of the authors (S.H.) was partially supported by KOSEF. This work was supported by U.S. Department of Energy Grant No. DE-FG02-01ER54628 and by Lawrence Livermore National Laboratory.

[1] H. M. Chung, B. A. Loomis, and D. L. Smith, J. Nucl. Mater. **239**, 139 (1996).
[2] S. J. Zinkle, H. Matsui, D. L. Smith, A. F. Rowcliffe, E. van Osch, K. Abe, and V. A. Kazakov, J. Nucl. Mater. **258–263**, 205 (1998).
[3] T. Diaz de la Rubia, H. M. Zbib, T. A. Khraishi, B. D. Wirth, M. Victoria, and M. J. Caturla, Nature (London) **406**, 871 (2000).
[4] E. E. Bloom, J. Nucl. Mater. **258–263**, 7 (1998).
[5] M. J. Mehl and D. A. Papaconstantopoulos Phys. Rev. B **54**, 4519 (1996).
[6] M. Mrovec, V. Vitek, D. Nguyen-Manh, D. Pettifor, and M. Sob, Mater. Res. Soc. Symp. Proc. **538**, 529 (1999).
[7] M. S. Daw and M. I. Baskes, Phys. Rev. B **29**, 6443 (1984).
[8] M. I. Baskes, Phys. Rev. B **46**, 2727 (1992).
[9] M. W. Finnis and J. E. Sinclair, Philos. Mag. A **50**, 45 (1984).
[10] M. M. Ali and R. Smith, Vacuum **44**, 377 (1993).
[11] R. Smith, Phys. Res. B **67**, 335 (1992).
[12] G. J. Ackland and M. W. Finnis, Philos. Mag. A **54**, 302 (1986).
[13] C. C. Matthai and D. J. Bacon, Philos. Mag. A **52**, 1 (1985).
[14] W. Maysenholder, R. Bauer, and A. Seeger, Phys. Lett. **109A**, 8 (1985).
[15] M. S. Daw and R. L. Hatcher, Solid State Commun. **56**, 697 (1985).
[16] M. S. Daw, M. I. Baskes, and W. G. Wolfer, in *Modeling Environmental Effects on Crack Processes*, edited by R. H. Jones and W. W. Gerberich (The Metallurgical Society, 1985).
[17] S. M. Foiles, Phys. Rev. B **32**, 7685 (1985).
[18] J. B. Adams and S. M. Foiles, Phys. Rev. B **41**, 3316 (1990).
[19] G. J. Ackland and R. Thetford, Philos. Mag. A **56**, 15 (1987).
[20] R. A. Johnson and W. D. Wilson, *Interatomic Potentials and Simulations of Lattice Defects* (Plenum, New York, 1972).
[21] F. W. Young, Jr., J. Nucl. Mater. **69/70**, 310 (1978).
[22] M. D. Johnson, M.-J. Caturla, and T. Diaz de la Rubia, J. Appl. Phys. **84**, 1963 (1998).
[23] C. Domain and C. S. Becquart, Phys. Rev. B **65**, 024103 (2001).
[24] J. Ihm, A. Zunger, and M. L. Cohen, J. Phys. C **12**, 4409 (1979).
[25] J. P. Perdew, K. Burke, and M. Ernzerhof, Phys. Rev. Lett. **77**, 3865 (1996).
[26] D. Vanderbilt, Phys. Rev. B **41**, 7892 (1990).
[27] S. G. Louie, S. Froyen, and M. L. Cohen, Phys. Rev. B **26**, 1738 (1982).
[28] S. Baroni, A. Dal Corso, S. de Gironcoli, and P. Giannozzi, http://www.pwscf.org.
[29] R. M. Wentzcovitch, Phys. Rev. B **44**, 2358 (1991).
[30] The WIEN97 code was used with the GGA functional.
[31] G. Bihlmayer, T. Asada, and S. Blügel, Phys. Rev. B **62**, R11937 (2000).
[32] *Handbook of Chemistry and Physics*, 81st ed. (Chemical Rubber, Cleveland, OH, 2000–2001).
[33] F. Birch, J. Geophys. Res. **57**, 227 (1952).
[34] B. B. Karki, G. J. Ackland, and J. Crain, J. Phys.: Condens. Matter **9**, 8579 (1997).
[35] W. Xu and J. A. Moriarty, Phys. Rev. B **54**, 6941 (1996).
[36] S. Dudarev (unpublished results).
[37] R. R. Coltman, Jr., C. E. Klabunde, J. K. Redman, and J. M. Williams, Radiat. Eff. **24**, 69 (1975).
[38] A. Satta, F. Willaime, and S. de Gironcoli, Phys. Rev. B **60**, 7001 (1999).
[39] A. Satta, F. Willaime, and S. de Gironcoli, Phys. Rev. B **57**, 11184 (1998).
[40] *Atomic Defects in Metals*, edited by H. Ullmaier, Landolt-Börnstein Series (Springer, Berlin, 1991), Vol. III/25.
[41] J. H. Rose, J. R. Smith, F. Guinea, and J. Ferrante, Phys. Rev. B **29**, 2963 (1984).
[42] G. J. Ackland, M. W. Finnis, and V. Vitek, J. Phys. F: Met. Phys. **18**, L153 (1988).
[43] G. J. Ackland, G. I. Tichy, V. Vitek, and M. W. Finnis, Philos. Mag. A **56**, 735 (1987).
[44] A. Machova and G. J. Ackland, Modell. Simul. Mater. Sci. Eng. **6**, 521 (1998).
[45] G. Simmons and H. Wang, *Single Crystal Elastic Constants and Calculated Aggregate Properties: A handbook* (MIT Press, Cambridge, 1971).
[46] The present GGA computation gives 5.72 eV as the cohesive energy of the bcc vanadium crystal.
[47] The first-principles value of 0.243 eV/atom is used.
[48] G. J. Ackland, D. J. Bacon, A. F. Calder, and T. Harry, Philos. Mag. A **75**, 713 (1997).
[49] L. A. Zepeda, S. Han, R. Car, D. J. Srolovitz, and B. D. Wirth (unpublished).
[50] J. F. Ziegler, J. P. Biersack, and U. Littmark, *The Stopping and Range of Ions in Solids* (Pergamon, New York, 1985).
[51] G. J. Ackland, *Alloy Modeling and Design* (The Metallurgical Society, Pittsburgh, 1993), p. 149.
[52] M. Born and K. Huang, *Dynamical Theory of Crystal Lattices* (Oxford University Press, Oxford, 1956).
[53] R. Colella and B. W. Batterman, Phys. Rev. B **1**, 3913 (1970).